PROCEEDINGS B

royalsocietypublishing.org/rspb

Research

Cite this article: Allemand R, Patterson E, Graboski R, Silcox MT, Herrel A. 2026 Endocranial morphology in worm lizards (Amphisbaenia, Squamata): multiple neuroanatomical solutions to a fossorial lifestyle. *Proc. R. Soc. B* **293**: 20260098.
https://doi.org/10.1098/rspb.2026.0098

Received: 14 January 2026
Accepted: 5 May 2026

Subject Category:
Morphology and biomechanics

Subject Areas:
ecology, biological applications, evolution

Keywords:
Amphisbaenia, Squamata, endocast, fossoriality, morphology, convergence, morphometric geometrics

Author for correspondence:
Rémi Allemand
e-mail: remi.allemand@gmail.com

Electronic supplementary material is available online at https://doi.org/10.6084/m9.figshare.c.8516961.

THE ROYAL SOCIETY PUBLISHING

Endocranial morphology in worm lizards (Amphisbaenia, Squamata): multiple neuroanatomical solutions to a fossorial lifestyle

Rémi Allemand[1], Elizabeth Patterson[2,3], Roberta Graboski[4], Mary Teresa Silcox[3] and Anthony Herrel[1,5,6,7]

[1]UMR 7179, Mécanismes Adaptatifs & Evolution (MECADEV), Muséum National d'Histoire Naturelle/CNRS, Paris, 75005, France
[2]Department of Biological Sciences, University of Manitoba, Winnipeg, Manitoba, Canada
[3]Department of Anthropology, University of Toronto Scarborough, Toronto, Ontario, Canada
[4]Coordenação da Zoologia, Museu Paraense Emílio Goeldi, Avenida Perimetral, 1900, Terra Firme, 66077-830, Belém, PA, Brazil
[5]Department of Biology, Evolutionary Morphology of Vertebrates, Ghent University, Ghent, Belgium
[6]Department of Biology, University of Antwerp, Wilrijk, Belgium
[7]Naturhistorisches Museum Bern, Bern, Switzerland

RA, 0000-0002-7912-7607; EP, 0009-0001-3071-5571; RG, 0000-0002-9123-4819; MTS, 0000-0002-4174-9435; AH, 0000-0003-0991-4434

Amphisbaenians are fossorial squamates characterized by extreme cranial specialization, particularly in snout morphology. Whether variation in external rostral form predicts internal cranial anatomy remains poorly understood. We present the first large-scale comparative analysis of amphisbaenian endocranial morphology, using three-dimensional landmark data from endocasts of 50 species representing all major families and snout morphotypes. Endocasts within Amphisbaenia share general squamate features typical of fossorial taxa. Phylogeny shows a weak but significant signal in endocast shape, while allometry shows no detectable effect. Snout morphology contributes modestly to endocranial variation, and substantial differences among taxa sharing the same snout shape indicate that anterior cranial modifications influence the braincase locally. Convergence and disparity analyses reveal limited, case-specific similarities across morphotypes, with similar endocranial configurations arising only sporadically in different lineages. Overall, amphisbaenian endocasts display considerable morphological variability and extreme snout modifications linked to digging performance do not produce a single, predictable endocranial configuration. These results suggest that endocranial shape reflects the interaction of multiple evolutionary factors. Future studies should explore additional sources of variation—such as ontogeny, sexual dimorphism, sensory biology, external forces or cranial musculature—to fully understand endocranial diversity in this clade.

1. Introduction

Convergent evolution has repeatedly produced similar phenotypes in distantly related taxa exposed to comparable selective pressures [1]. These recurrences highlight the interplay between determinism and constraint in adaptive evolution [2]. Phenotypic similarities, especially when associated with specific microhabitats, are often driven by the functional and ecological demands of those environments. A striking example is the evolution of fossoriality, defined as the capacity to move and carry out most daily activities

below ground. This lifestyle, together with the different habitats and substrate types associated [3], generates distinct selective pressures that have repeatedly driven convergent changes in morphology, behaviour and physiology across diverse vertebrate clades (e.g. [4,5]).

Among squamates, fossoriality has evolved independently in multiple lineages across different continents [6], leading to marked convergence in external morphology, locomotion, diet, reproductive strategies and physiology [7–10]. Cranial architecture, in particular, is profoundly modified in fossorial squamates: skull miniaturization, fusion of cranial elements and specialized head morphologies are common features of species adapted to digging and are thought to have evolved in response to the physical properties of head-first burrowing in different substrates [11,12]. However, these cranial modifications likely evolve under multiple, and often competing, selective pressures, which generally result in functional and ecological trade-offs. For instance, adaptations that enhance burrowing performance—such as efficient underground locomotion, friction reduction and the ability to penetrate compacted soils—can simultaneously reduce bite force, thereby restricting dietary breadth and reinforcing ecological specialization [3,13]. These trade-offs illustrate how environmental demands on the skull can lead to broader ecological consequences, shaping not only the mechanics of burrowing but also recurrent patterns of ecological specialization and morphological convergence across fossorial squamates.

While external cranial morphology in squamates has been extensively studied in the context of fossorial adaptations, the potential impact of fossoriality on internal cranial structures remains largely unexplored. Most comparative studies addressing this topic have so far focused on inner ear morphology [14–19], revealing some convergent traits—such as a globular vestibule and reduced semicircular canals—but with a weak overall signal once phylogeny and allometry are accounted for [16]. Beyond the inner ear, the degree to which fossoriality may have impacted other cranial internal structures such as the brain remains poorly understood. A few studies on squamate brain and endocast anatomy have described recurring neuroanatomical features in fossorial taxa [20–24], suggesting patterns that may be associated with a subterranean lifestyle. However, these studies either focus exclusively on snakes [20,24] or include a limited subset of squamate clades that have independently evolved a fossorial lifestyle [21–23]. As a result, the extent to which fossorial lifestyles may have driven convergent changes in squamate neuroanatomy remains largely unknown.

This study aims to investigate neuroanatomical modifications associated with selective pressures related to fossoriality in a specific clade of squamates, Amphisbaenia, commonly known as worm lizards [25]. Amphisbaenians offer a compelling model due to their extreme morphological specializations for subterranean life. Currently, this clade is widely considered to be monophyletic, placed as the sister group of lacertid lizards [26], and divided into six families (Amphisbaenidae, Blanidae, Bipedidae, Cadeidae, Rhineuridae and Trogonophidae) [25,27–29]. As obligate head-first burrowers, amphisbaenians display profound anatomical adaptations to fossoriality, including elongated bodies, the loss of limbs (except in *Bipes*), rudimentary eyes, and the absence of external ears [25,30]. Their skulls are highly modified for digging through soil and fall into four main morphotypes (round-, shovel-, keel- and spade-snouted), each having been suggested to be associated with distinct burrowing mechanics [31]. With the exception of the spade-snouted Trogonophidae, these morphotypes are not monophyletic but have evolved independently multiple times, often in response to substrate type [32].

Here, we used endocasts (i.e. casts of the brain cavity) as proxies for the external morphology of the brain to investigate the impact of selective pressures associated with digging performance on internal cranial structures within Amphisbaenia. In amphisbaenians, the braincase is nearly fully ossified [21], providing a clear delimitation of the endocast and enabling precise morphological comparisons. By using landmark-based geometric morphometrics, we quantitatively compared the endocasts of different amphisbaenian species to determine whether variation in rostral morphology leads to changes in more posterior cranial regions. Because snout morphology in amphisbaenians is closely linked to distinct digging behaviours, which may impose functional constraints on skull architecture, we predict that species sharing similar snout morphotypes may exhibit similar endocranial configurations and potentially display signals of morphological convergence. Our analyses aim to uncover the factors shaping endocast morphology in this clade and to test whether the patterns observed in other squamates—particularly the influence of phylogeny and size—also apply to amphisbaenians.

2. Material and methods

(a) Specimen sampling and data acquisition

Fifty species of the clade Amphisbaenia (see table 1 and figure 1) were selected to perform endocast comparisons. The dataset captures the taxonomic diversity of the clade, one specimen per species, and includes the different snout morphotypes (i.e. round, spade-, keel- and shovel-snouted shapes) documented across amphisbaenians [7,29]. In this study, we use the term *snout* rather than *head* to refer to these morphotypes. Although both terms are used in the literature, we favour *snout*, as our objective is to assess whether the functional pressures shaping the snout also influence more posterior cranial regions, with endocast morphology serving as a proxy for these regions. Endocranial regions are identified based on the soft tissues they overlie (e.g. 'cerebral hemispheres'), rather than simply as impressions of these structures.

Computed tomographic scans of these species were gathered from multiple sources (see table 1). Scans for 45 specimens were acquired from the online repository MorphoSource [34] (http://www.MorphoSource.org). In addition, five specimens were acquired by one of the co-authors (A.H.) and scans were performed at the Centre for X-Ray Tomography at Ghent University, Belgium (UGCT; https://www.ugent.be/we/ugct/en) using the HECTOR µCT scanner [35] and at the European Synchrotron Radiation Facility (ESRF, Grenoble, France) using third-generation synchrotron microtomography on beamlines ID19 and BM5. Scanning parameters were sample-dependent, with tube voltages ranging from 100 to 120 kV and a tube current of

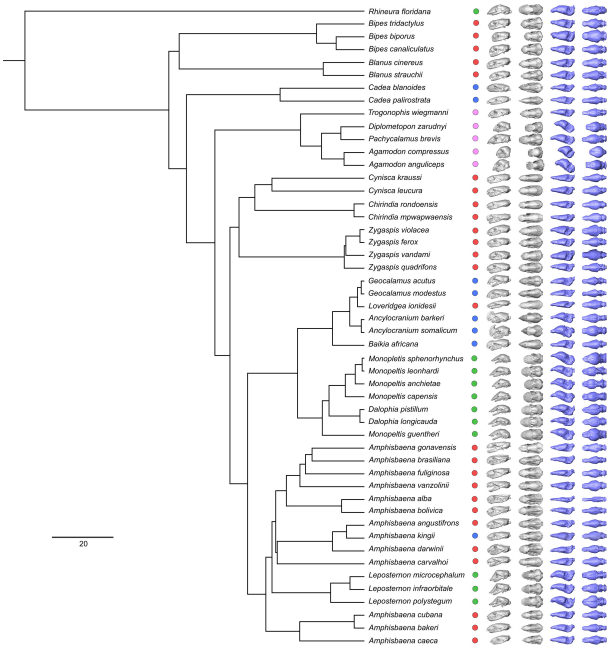

Figure 1. Phylogenetic relationships of amphisbaenians sampled in the study (modified from [29]) associated with 3D renderings showing the skull and endocast in left lateral and dorsal views. Circles next to species names are colour-coded according to snout shape categories: round (red), keel (blue), shovel (green) and spade (pink). Branch lengths indicate genetic divergence; scale bar = 20 units.

approximately 150 µA. Datasets were reconstructed from cone-beam acquisitions over 360° using Octopus Reconstruction v. 8.9.4.2 and filtered back-projection algorithm with the ESRF PYHST software.

Image segmentation and visualization were carried out in Avizo v. 2019.1 (Thermo Fisher Scientific, Waltham, MA, USA). Using the segmentation tools, the endocast of each species was manually reconstructed by delineating the internal surface of the bones enclosing the endocranial cavity. All resulting surface volume files for the segmented endocasts are available on MorphoSource under the project name 'Amphisbaenian endocasts' (https://www.morphosource.org/projects/000839453?locale=en).

(b) Landmarks and statistical analysis

The landmarking protocol established by [36] was applied to compare endocast morphologies. Nineteen of the twenty landmarks defined in that study were selected, as landmark 8 ('*most ventro-median extent of the endocast at the posterior margin of the optic nerve foramen*') could not be consistently located across amphisbaenians. All landmarks were positioned on the virtual endocasts and exported using the software Avizo (see electronic supplementary material, data S1 for the list and positions of landmarks).

Endocast shape variation was quantified using a generalized procrustes analysis (GPA) performed with the *gpagen* function in the R package 'geomorph' [37]. Patterns of endocranial shape variation were explored using phylogenetic principal components analysis (pPCA) under a Brownian motion model with the *phyl.pca* function in 'phytools' [38]. Analyses were conducted on the raw dataset, with interpretation focusing on axes explaining at least 10% of the total variance. To visualize size-independent shape variation, a pPCA was also performed on allometry-corrected shape data (see below and electronic supplementary material, data S2). A standard PCA (*gm.prcomp*; 'geomorph') was additionally performed on raw shape data (electronic supplementary material, data S3) to provide a complementary visualization of morphological variation independent of phylogenetic structure.

The phylogenetic signal associated with endocast morphology was assessed using the multivariate K-statistic with the *physignal* function in 'geomorph' [39]. The phylogenetic tree used for these analyses was taken from [29] and applied without modification to its topology or branch lengths (see figure 1). To quantify the evolutionary independence of snout morphotypes, we first estimated the minimum number of transitions using *parsimony* ('phangorn' [40]) and then performed stochastic character mapping with 100 simulations under an equal-rates model ('phytools' [38]).

To evaluate the influence of snout shape on amphisbaenian endocast morphology while accounting for allometry (i.e. log-transformed centroid size), a phylogenetic MANCOVA was conducted using the *mvgls* and *manova.gls* functions in the R package 'mvMORPH' [41]. The analysis tested the effects of snout shape, centroid size, and their interaction on multivariate shape, with statistical significance assessed using Pillai's trace. Pairwise *post hoc* comparisons among snout morphotypes were performed using *pairwise.glh* (1000 permutations, Holm correction [42]). To characterize shape variation independent of size, a phylogenetic multivariate regression of endocast shape on log-transformed centroid size was performed using *mvgls*. Residuals from this regression were extracted and used as input for a phylogenetic principal component analysis to visualize allometry-corrected morphological variation (see electronic supplementary material, data S2).

The diversity in endocast morphology among amphisbaenians with diverse snout shapes was assessed through morphological disparity analyses. Two complementary metrics were calculated using the first 13 pPCA axes, which together account for approximately 95% of the total shape variance derived from the generalized Procrustes-aligned landmarks: (i) the sum of

Table 1. Amphisbaenia species analysed. See institutional abbreviations for collection numbers. AH, coauthor's personal collection. Ab., Species name abbreviations used in electronic supplementary material, data S2, S3 and S5. A double dagger (‡) indicates specimens generated by the oVert Project [33]. An asterisk (*) indicates specimens not coming from the MorphoSource database. Institutional abbreviations: CAS, California Academy of Science, San Francisco, California, USA; FMNH, The Field Museum of Natural History, Chicago, Illinois, USA; MCZ, Museum of Comparative Zoology, Harvard University, Cambridge, Massachusetts, USA; MNHN, Muséum National d'Histoire Naturelle, Paris, France; MVZ, Museum of Vertebrate Zoology, University of California, Berkeley, USA; UF, The University of Florida, Gainesville, Florida, USA; UMMZ, University of Michigan Museum of Zoology, Ann Arbor, Michigan, USA; YPM, Yale Peabody Museum, New Haven, Connecticut, USA.

family	species	Ab.	collection number	voxel size (mm)	snout shape
Rhineuridae	*Rhineura floridana*	Ri.f	YPM:VZ:YPM HERR 001213‡	0.032	shovel
Bipedidae	*Bipes tridactylus*	Bi.t	MCZ:Herp:R-145817	0.026	rounded
	Bipes biporus	Bi.b	UF:Herp:42060‡	0.009	
	Bipes canaliculatus	Bi.c	MVZ:Herp:MVZ:Herp:240726‡	0.033	
Blanidae	*Blanus cinereus*	Bl.c	FMNH:Amphibians and Reptiles:603‡	0.014	rounded
	Blanus strauchii	Bl.s	AH*	0.014	
Cadeidae	*Cadea blanoides*	Ca.b	MVZ:Herp:MVZ:Herp:241291‡	0.029	keel
	Cadea palirostrata	Ca.p	MCZ:Herp:R-12088	0.026	
Trogonophidae	*Trogonophis wiegmanni*	Tr.w	MVZ:Herp:MVZ:Herp:250710‡	0.029	spade
	Agamodon anguliceps	Ag.a	FMNH:Amphibians and Reptiles:264702‡	0.053	
	Agamodon compressus	Ag.c	MCZ:Herp:R-66455‡	0.011	
	Pachycalamus brevis	Pa.b	MVZ:Herp:MVZ:Herp:236445‡	0.033	
	Diplometopon zarudnyi	Di.z	FMNH:Amphibians and Reptiles:64 429	$x, y = 0.009$ $z = 0.019$	
Amphisbaenidae	*Zygaspis ferox*	Zy.f	MCZ:Herp:R-182217‡	0.019	rounded
	Zygaspis quadrifons	Zy.q	CAS:Herp:159076‡	0.028	
	Zygaspis vandami	Zy.va	MCZ:Herp:R-184523	0.022	
	Zygaspis violacea	Zy.vi	MCZ:Herp:R-14199	0.022	
	Chirindia mpwapwaensis	Ch.m	MCZ:Herp:R-30767‡	0.011	
	Chirindia rondoensis	Ch.r	MCZ:Herp:R-59173	0.015	
	Cynisca kraussi	Cy.k	MCZ:Herp:R-55189	$x, y = 0.022$ $z = 0.017$	
	Cynisca leucura	Cy.l	YPM:VZ:YPM HERR 008119‡	0.028	
	Geocalamus acutus	Ge.a	AH*	0.014	keel
	Geocalamus modestus	Ge.m	MCZ:Herp:R-18294	0.022	
	Loveridgea ionidesii	Lo.i	MCZ:Herp:R-50019	$x, y = 0.022$ $z = 0.017$	rounded
	Baikia africana	Ba.a	FMNH:Amphibians and Reptiles:265090‡	0.017	keel
	Ancylocranium barkeri	An.b	MCZ:Herp:R-67004‡	0.007	
	Ancylocranium somalicum	An.s	FMNH:Amphibians and Reptiles:265051‡	0.035	
	Monopeltis guentheri	Mo.g	MCZ:Herp:R-8980‡	0.019	shovel
	Monopeltis capensis	Mo.c	UMMZ:herps:181690‡	0.029	
	Monopeltis leonhardi	Mo.l	MCZ:Herp:R-150042	0.026	
	Monopeltis anchietae	Mo.a	YPM:VZ:YPM HERR 001639‡	0.040	
	Monopeltis sphenorhynchus	Mo.s	UMMZ:herps:181691‡	0.029	
	Dalophia longicauda	Da.l	MCZ:Herp:R-150031	0.022	
	Dalophia pistillum	Da.p	UMMZ:herps:181692‡	0.035	
	Amphisbaena cubana	A.cu	MCZ:Herp:R-162424	0.026	rounded
	Amphisbaena bakeri	A.ba	MCZ:Herp:R-66512	0.024	
	Amphisbaena caeca	A.ca	MCZ:Herp:R-58831	0.024	
	Leposternon polystegum	Le.p	MCZ:Herp:R-3359	0.022	shovel
	Leposternon infraorbitale	Le.i	MCZ:Herp:R-98292	0.034	
	Leposternon microcephalum	Le.m	MCZ:Herp:R-20624‡	0.014	

(*Continued.*)

Table 1. (*Continued.*)

family	species	Ab.	collection number	voxel size (mm)	snout shape
	Amphisbaena kingii	A.ki	AH*	0.005	keel
	Amphisbaena angustifrons	A.an	UF:Herp:141551‡	0.018	rounded
	Amphisbaena darwinii	A.da	UF:Herp:141549‡	0.009	
	Amphisbaena alba	A.al	FMNH:Amphibians and Reptiles:195924‡	$x, y = 0.022$ $z = 0.053$	
	Amphisbaena bolivica	A.bo	UF:Herp:141550‡	0.010	
	Amphisbaena carvalhoi	A.car	MCZ:Herp:R-128421	0.015	
	Amphisbaena gonavensis	A.go	AH*	0.007	
	Amphisbaena vanzolinii	A.va	MNHN 1998.02.02*	0.007	
	Amphisbaena fuliginosa	A.fu	MCZ:Herp:R-24003‡	0.019	
	Amphisbaena brasiliana	A.br	MCZ:Herp:R-36945	0.034	

variances, representing the overall spread of taxa in morphospace, and (ii) the functional divergence, reflecting the extent to which taxa occupy peripheral regions of morphospace relative to the group centroid [43]. Disparity metrics were estimated using the *dispRity.per.group* function in the R package 'dispRity' [44]. Differences in disparity among snout morphotypes were statistically assessed with Bhattacharyya distances using the *test.dispRity* function in 'dispRity' [44], which evaluates the degree of overlap between distributions of disparity values [45].

Convergence in endocast morphology among amphisbaenians sharing similar snout morphologies was assessed using the angle-based method implemented in the *search.conv* function of the R package 'RRphylo' [46]. This approach evaluates whether taxa with a predefined state—in this case, snout morphology—are more similar in multivariate trait space than expected based on their phylogenetic relationships, using angular distances among phenotypes [47]. Analyses were conducted on the first 13 pPCA axes, which together accounted for approximately 95% of total variance in raw endocast shape data. Convergence was tested across morphotypes and within each morphotype, except for the 'spade' shape, which was excluded because it forms a monophyletic group (Trogonophidae [32]). The function evaluates convergence by measuring mean angular distances between taxa sharing a state and their closest phenotypic neighbours, considering both observed trait values (*ang.state*) and inferred evolutionary timing (*ang.state.time*). Convergence is significant when observed similarity exceeds that expected under a neutral Brownian-motion model (using 1000 simulations).

To complement this angle-based approach, phenotypic convergence was also quantified using the distance-based C-metrics framework (C1–C4) [1]. These metrics, implemented in the R package 'convevol', quantify the extent to which lineages have evolved closer to each other in phylomorphospace relative to their maximum historical divergence [1]. Statistical significance was assessed by comparing observed values with those obtained from simulations under a Brownian-motion model of trait evolution using the *convSig* function (1000 simulations). As in the RRphylo analyses, calculations were performed on the first 13 pPCA axes explaining approximately 95% of total shape variance to reduce dimensionality while retaining most morphological information.

3. Results

(a) Descriptions of amphisbaenian endocasts

In most amphisbaenians, the morphology of the endocast is typical of that of non-avian reptiles [48] in that it exhibits a tubular shape that is longer than wide and has a smooth surface (figure 1; electronic supplementary material, data S4 for labelled endocasts). In lateral view, cephalic and pontine flexures vary among species, ranging from a nearly straight endocast (e.g. *Amphisbaena angustifrons*; figure 1; electronic supplementary material, data S4) to a more flexed structure (e.g. *Leposternon polystegum*; figure 1; electronic supplementary material, data S4), in which the different regions are not fully aligned in the horizontal plane. The most extreme flexures occur in the genus *Agamodon*, with the deep-burrowing *A. compressus* exhibiting a short and rounded endocast that differs markedly from the typical amphisbaenian pattern (figure 1; electronic supplementary material, data S4).

Anteriorly, the olfactory bulbs and peduncles in amphisbaenians are relatively short and thick (figure 1; '*olf*' in electronic supplementary material, data S4), with variable antero-posterior length ranging from a very short (e.g. *L. polystegum*; electronic supplementary material, data S4) to a more elongated structure (e.g. *A. angustifrons*; electronic supplementary material, data S4). The outer shape of the endocast does not offer sufficient detail to clearly distinguish the olfactory bulbs from the peduncles. Depending on the species, a slight groove on the dorsal surface of the endocast may, or may not, indicate the medial limit between the paired olfactory bulbs and peduncles (see '*olf.gr*' in electronic supplementary material, data S4). In lateral view, the olfactory bulbs and peduncles can be aligned with the rest of the endocast (e.g. *A. angustifrons*; electronic supplementary material, data S4), or projected more ventrally (e.g. *Dalophia longicauda*; electronic supplementary material, data S4).

Posterior to the olfactory peduncles, the cerebral hemispheres expand laterally and ventrally to form the largest part of the amphisbaenian endocast (figure 1; '*cer*' in electronic supplementary material, data S4). The anterior and posterior limits

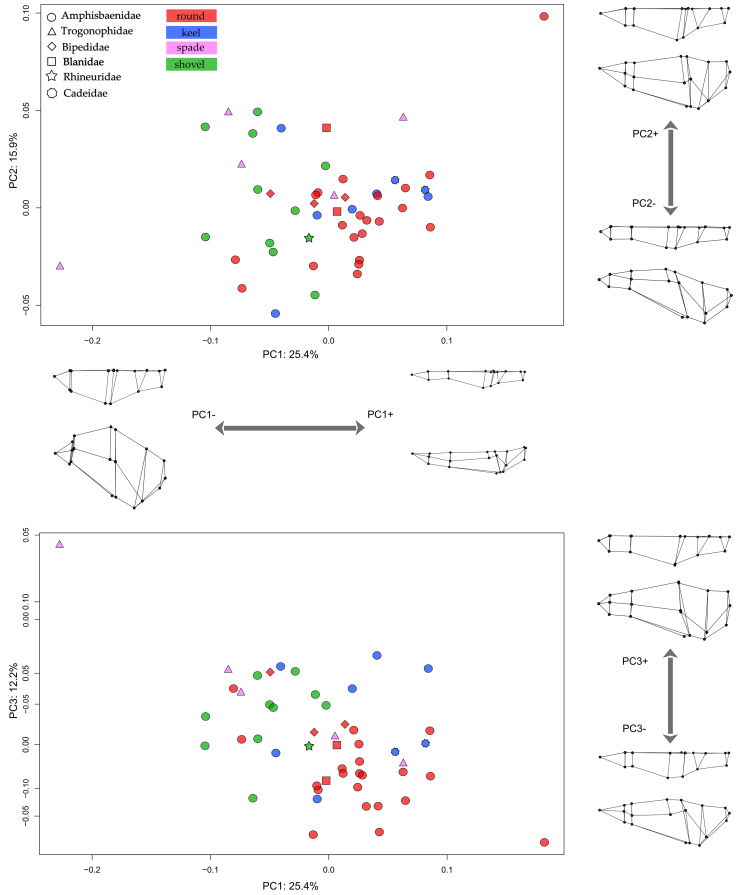

Figure 2. Phylomorphospaces of amphisbaenian endocast shape coloured by snout type. The first three principal components (PC1–PC3) are shown. Wireframes represent reconstructed landmark configurations corresponding to the extremes of each PC axis, in dorsal (top) and lateral (bottom) views. A version of the figure with full species labels is provided in electronic supplementary material, data S5.

of the cerebral hemispheres are difficult to locate and indicated only by changes in the width of the endocast (figure 1; electronic supplementary material, data S4). In dorsal view, the cerebral hemispheres in amphisbaenians reach their maximal width in their posterior part. A groove on the surface of the endocast indicates the position of the interhemispheric fissure that runs between the paired cerebral hemispheres (e.g. *Bipes biporus*; '*inter.f*' in electronic supplementary material, data S4). In some amphisbaenians (e.g. *A. angustifrons*; electronic supplementary material, data S4), such a groove is poorly defined on the endocast, and the dorsal surface of the cerebral hemispheres is smooth. In lateral view, the cerebral hemispheres in amphisbaenians exhibit an ovoid, tubular shape, distinct from the rest of the endocast (figure 1; electronic supplementary material, data S4). They are oriented either along the same axis as the rest of the endocast (e.g. *A. angustifrons*; electronic supplementary material, data S4) or variably inclined dorsoventrally along their anteroposterior length (e.g. *L. polystegum;* electronic supplementary material, data S4).

Postero-ventral to the cerebral hemispheres, the ventral diencephalon forms a bulge on the ventral surface of the endocast in most amphisbaenians, differing in size depending on species (figure 1; '*dienc*' in electronic supplementary material, data S4). In some amphisbaenians, this bulge is small and the ventral diencephalon is difficult to locate on the endocast (e.g. *B. biporus*; electronic supplementary material, data S4). Posterior to the cerebral hemispheres, the optic tectum and cerebellum in amphisbaenians are not distinguishable from the rest of the endocast. Their position is inferred only by a marked change in endocast width, relative to the cerebral hemispheres and by the large, round impressions of the endosseous labyrinth on the postero-lateral surfaces of the endocast ('*lab*' in electronic supplementary material, data S4). On the postero-ventral part of the amphisbaenian endocast, the medulla oblongata ('*mo*' in electronic supplementary material, data S4) forms a wide, ventrally convex arc and exhibits a pontine flexure of variable degree depending on the species (figure 1; electronic supplementary material, data S4). It projects dorsally to meet the spinal cord at the level of the foramen magnum. However, the rounded impressions of the endosseous labyrinth on the lateral surface of the endocast prevent a precise delineation of its boundaries (figure 1 and electronic supplementary material, data S4).

(b) Morphospace distributions and statistical results

The pPCA indicates that the first three axes account for 53.4% of total endocast shape variance (PC1 = 25.4%, PC2 = 15.9%, PC3 = 12.2%; figure 2; see electronic supplementary material, data S5 for remaining PCs and for the pPCA with labels).

PC1 captures variation in dorsoventral compression and cephalic flexure of the endocast (figure 2). Taxa with high PC1 scores exhibit flattened endocasts with reduced flexure, whereas those with low scores show taller, more expanded endocasts with pronounced cephalic flexure. Shovel-snouted species are restricted to negative PC1 values, while spade-snouted taxa occur

Table 2. Results of the phylogenetic MANCOVA (Pillai's test). The values in bold denote statistically significant results.

	Pillai's test	Pr(>Stat)
snout-shape	2.27	**0.001**
log(GPA$Csize)	0.57	0.58
snout-shape :centroid size	1.59	0.76

Table 3. *Post hoc* pairwise contrasts among snout morphotypes from the phylogenetic MANCOVA of endocast shape (centroid size as covariate). The significance test was based on 1000 iterations.

pairwise comparisons		
	Pillai's trace	*adjusted p-value*
keel : round	0.45	1
keel : shovel	0.56	1
keel : spade	0.74	0.11
round : shovel	0.42	1
round : spade	0.67	0.63
shovel : spade	0.63	1

across both sides of the axis (figure 2). Most round- and keel-snouted taxa occupy positive PC1 values. At the family level, Blanidae and Cadeidae are confined to positive scores, whereas other families span both sides, with Amphisbaenidae and Trogonophidae showing the greatest dispersion.

PC2 reflects variation in the relative size, elongation and dorsoventral position of the anterior endocast (figure 2). Taxa with low PC2 scores exhibit shorter olfactory peduncles and bulbs positioned more ventrally, with the greatest lateral extent occurring anteriorly. In contrast, taxa with high PC2 scores show elongated olfactory structures positioned more dorsally, and the point of maximum lateral width shifts posteriorly along the olfactory peduncles. Most spade-snouted trogonophids occupy positive PC2 values, whereas other snout categories are distributed across both sides of the axis. Amphisbaenidae display the widest distribution along PC2, while Cadeidae and Bipedidae are more restricted to positive values.

PC3 mainly reflects variation in the posterior part of the endocast and in the position of maximum cerebral hemispheric width (figure 2). Taxa with positive PC3 scores exhibit a posteriorly positioned maximum width and a relatively tall posterior end, whereas taxa with negative scores show maximum width at mid-hemisphere and a posterior region that narrows markedly in height. Round-snouted taxa occur predominantly on the negative side of PC3, although some overlap exists. Most shovel- and spade-snouted taxa occupy positive values, while keel-snouted taxa are distributed across both sides. At the family level, Trogonophidae show the broadest distribution and are predominantly positive, Bipedidae are restricted to positive values, Blanidae and Cadeidae occur only on negative values, and Amphisbaenidae span both sides of the axis.

Endocranial shape variation in extant amphisbaenians shows a significant phylogenetic signal (K-mult = 0.16, p = 0.007, ZCR = 3.61). However, the low K value indicates that phylogenetic structuring of shape is weak despite this statistical significance. Parsimony reconstruction indicated a minimum of eight independent transitions among snout morphotypes. Stochastic mapping estimated a mean of 9.8 transitions under an equal-rates model. This relatively high number of transitions suggests that the different snout morphotypes evolved repeatedly within Amphisbaenia, providing a suitable framework to test potential associations between snout morphology and endocast shape.

The phylogenetic MANCOVA using Pillai's trace revealed a significant effect of snout shape on endocast morphology (p < 0.001; table 2). In contrast, log-transformed centroid size explained only a small proportion of shape variation (R^2 = 0.036) and was not statistically significant (p = 0.058), and the interaction between snout shape and size was also non-significant (p = 0.764; table 2). *Post hoc* pairwise comparisons based on 1000 permutations with Holm correction revealed no significant differences between any pairs of snout morphotypes (see table 3). These results indicate that endocast shape variation is influenced by snout morphotype at the global model level, when accounting for phylogeny and centroid size. However, the absence of significant pairwise contrasts after correction suggests that morphological differences among specific morphotype pairs are moderate and partially overlapping rather than sharply distinct. Additionally, centroid size has a weak and non-significant effect on shape, and there is no evidence that allometric trajectories differ among morphotypes.

When using the *sum of variances* as a metric of endocast morphological disparity, the four snout shape categories exhibited comparable levels of variation, with overlapping confidence intervals across all groups, indicating similar overall morphospace volumes occupied (see table 4; electronic supplementary material, data S6). Spade-snouted amphisbaenians display the highest observed disparity, whereas keel-, shovel- and round-snouted taxa show lower, roughly comparable values (table 4). Overlapping 95% bootstrap confidence intervals suggest that these differences are not statistically significant (electronic supplementary material, data S6). Pairwise comparisons using Bhattacharyya coefficients indicate generally higher similarity among keel, round and shovel-snouted taxa, whereas spade-snouted taxa show lower overlap with the other groups (electronic supplementary material, data S6), consistent with both higher disparity and greater morphological distinctiveness of this group.

When the metric *functional divergence* is considered (see electronic supplementary material, data S6), the spade-snouted amphisbaenians display the highest divergence (table 4), indicating that this group includes more extreme endocast

Table 4. Endocast morphological disparity indices (sum of variances and functional divergence) across snout morphotypes of amphisbaenians.

snout shape	*N*	sum of variances	functional divergence
keel	8	0.009	0.082
round	26	0.007	0.069
shovel	11	0.009	0.091
spade	5	0.022	0.102

Table 5. Convergence results as returned by the function *search.conv* and tested (i) across snout morphologies and (ii) within each morphotype, except for the 'spade' shape. The significance test was based on 1000 iterations. The values in bold denote statistically significant results.

(i) state	ang.state	p.ang.state	ang.state.time	p.ang.state.time
round : keel	85.5	**0.005**	1.28	0.45
round : shovel	105.9	1	1.28	0.31
round : spade	102.4	1	1	0.08
keel : shovel	95.5	0.99	1.38	0.66
keel : spade	86.4	0.23	0.84	**0.009**
shovel : spade	66.5	**0.001**	0.63	**0.001**

(ii) state	ang.state	p.ang.state	ang.state.time	p.ang.state.time
round	79.52	**0.001**	1.17	0.17
keel	67.88	**0.006**	2.16	0.92
shovel	60.39	**0.001**	2.58	1

morphologies deviating from the group centroid. Shovel- and keel-snouted taxa show intermediate divergence, while round-snouted species display the lowest divergence (table 4). Despite these numerical differences, the overlapping confidence intervals again suggest no statistically significant differences in the extent to which species deviate from their group centroid. Pairwise Bhattacharyya coefficients reveal that keel-snouted taxa are highly similar to both round- and shovel-snouted groups, whereas spade-snouted taxa display lower overlap with all other groups (electronic supplementary material, data S6), reflecting their greater morphological distinctiveness. Round- and shovel-snouted taxa also show moderately low overlap (electronic supplementary material, data S6), indicating some divergence between these two groups as well. Overall, these results indicate that, while all snout morphotypes occupy broadly similar morphospace in terms of deviation from their group centroids, spade-snouted taxa encompass a higher proportion of extreme morphologies, and subtle differences exist between round- and shovel-snouted endocasts.

Using *search.conv*, we tested for convergence in endocast shape among amphisbaenians grouped by snout morphology (table 5). Across morphotypes, pairwise comparisons based on raw phenotypic angles (*ang.state*) indicate significant convergence between round- and keel-snouted taxa and between shovel- and spade-snouted taxa, compared to expectations under a Brownian motion model, while other pairings were non-significant (table 5(i)). When branch lengths are incorporated (*ang.state.time*), significant convergence is detected for keel versus spade and shovel versus spade, with all other pairings remaining non-significant (table 5(i)). Within morphotypes, mean angles suggest some convergence using the raw metric, but *ang.state.time* shows no significant within-morphotype convergence (table 5(ii)).

Phenotypic convergence assessed using the C-metrics framework (C1–C4) reveals limited evidence of significant convergence among most snout morphotypes (table 6). Significant convergence was detected only in comparisons involving the spade morphotype. Specifically, round-spade and shovel-spade pairs showed significant reductions in phenotypic distance relative to their maximum historical divergence (table 6). No other morphotype comparisons were significant for C1 or C2, and the C3 and C4 metrics were not significant for any pair (table 6). Overall, the angle-based and distance-based approaches reveal broadly consistent patterns of limited convergence in endocast shape among snout morphotypes. Both methods identify significant convergence only in a few pairwise comparisons, with the most consistent signal observed between shovel- and spade-snouted taxa. Other morphotype pairs show either weak or method-specific signals of convergence, and no convergence is detected within morphotypes when evolutionary time is taken into account. Together, these results suggest that similarities in endocast morphology among amphisbaenians occur only in a limited number of cases rather than representing a widespread pattern across snout types.

4. Discussion

This study provides the first large-scale comparative analysis of endocast morphology in Amphisbaenia, a clade of highly specialized fossorial squamates. Amphisbaenian endocasts are characterized by short and stout olfactory bulbs and peduncles, tubular cerebral hemispheres, flattening of the ventral diencephalon, and a weak distinction of both the optic tectum and the

Table 6. Pairwise phenotypic convergence (C1–C4) among amphisbaenian snout morphotypes. Numbers in parentheses are *p*-values and significant values are shown in bold.

pair	C1	C2	C3	C4
round : keel	0.07 (0.18)	0.01 (0.07)	0.03 (0.39)	0.0003 (0.30)
round : shovel	0.06 (0.31)	0.01 (0.06)	0.03 (0.53)	0.0003 (0.37)
round : spade	0.09 (**0.04**)	0.01 (**0.007**)	0.04 (0.104)	0.0004 (0.20)
keel : shovel	0.04 (0.69)	0.007 (0.17)	0.02 (0.90)	0.0001 (0.95)
keel : spade	0.06 (0.38)	0.01 (0.08)	0.03 (0.47)	0.0005 (0.20)
shovel : spade	0.12 (0.02)	0.02 (**0.0001**)	0.05 (0.07)	0.0004 (0.44)

Note: Significance test was based on 1000 iterations.

cerebellum. These neuroanatomical features are consistent with general patterns observed in fossorial squamates [20,22,24]. However, substantial variability is evident among species, expressed in traits such as the degree of cephalic and pontine flexures, the elongation and orientation of the olfactory bulbs and peduncles, the shape and position of the cerebral hemispheres, and the flexure of the medulla oblongata. Together, these differences indicate considerable morphological variability in the endocranial anatomy of amphisbaenians.

Our results show that this interspecific endocranial variability is influenced in part by phylogeny. However, similar to previous studies on squamate endocasts [20,48], the low K statistic indicates that phylogenetic structuring is weak, despite being statistically significant. In addition, log-transformed centroid size, used as a proxy for size, explained only a small portion of shape variation and was not statistically significant, suggesting that allometric scaling plays a limited role in shaping endocranial morphology in amphisbaenians. This contrasts with findings in other squamates, where size has been identified as a major driver of endocranial shape [48,49], a difference that could be related to the generally small head size of amphisbaenians [25,30,31].

Beyond size and phylogeny, snout morphology appears to contribute to certain aspects of endocranial variation, although its effects are subtle. In amphisbaenians, snout morphotypes are intimately related to different patterns of excavation and compacting behaviour, which range from non-directed movements of the head (round-snouted morphotype) and lateral movements (keel-snouted) to shovelling (shovel-snouted) and screwing (spade-snouted) movements [7,30]. Given these strong functional links, one might expect rostral specializations to consistently influence endocast morphology, either through biomechanical constraints associated with digging performance or through developmental integration between the rostrum and the braincase. When both size and phylogeny are accounted for, the phylogenetic MANCOVA revealed a significant global effect of snout shape on endocast morphology. However, *post hoc* pairwise comparisons show no statistically significant differences between morphotypes after correction, indicating that differences among specific morphotype pairs are moderate and partially overlapping. Overall, these results suggest that rostral specializations may indirectly influence the posterior skull (i.e. the braincase) and thus modulate endocast morphology in amphisbaenians, although this influence remains limited and does not produce clearly distinct endocranial configurations among snout morphotypes.

Disparity analyses further support the subtlety of this snout-endocast relationship. Although spade-snouted taxa occupy a slightly larger region of morphospace, the extensive overlap of confidence intervals among snout morphotypes indicates that endocranial variation, similar to the pattern documented in the atlantoaxial complex [50], is not strictly dictated by snout type. Even the most specialized morphotype, such as the shovel snout, adapted for penetrating compacted soils [30,31], does not display distinctive endocasts compared with other amphisbaenians, suggesting that even extreme cranial adaptations do not necessarily produce a unique endocast morphology. Convergence analyses reveal limited and inconsistent signals of convergence among morphotypes: significant convergence was detected only in a few pairwise comparisons, most consistently involving shovel- and spade-snouted taxa, whereas other pairs show weak or method-specific signals. Similar endocranial configurations can sporadically arise in different lineages with different morphotypes, but such instances are rare and do not represent a general pattern.

Overall, these results indicate that similar rostral morphologies do not consistently lead to convergent endocranial configurations. Even in cases of extreme snout specialization, such as the spade-snouted trogonophids, adapted for torsional-burrowing movements [7], the effects of cranial modifications on endocast morphology are largely local and do not substantially alter overall shape. For instance, in *D. zarudnyi*, *A. anguliceps* and *A. compressus*, pronounced cranial angulation and shortening produce strongly flexed endocasts. This pattern contrasts with the two other spade-snouted trogonophids, *Trogonophis wiegmanni* and *Pachycalamus brevis*, which maintain a more typical endocranial configuration despite sharing the same snout morphology. These results suggest that snout shape, together with the digging performance associated with each morphotype, acts as one of several interacting factors shaping endocast morphology rather than as a deterministic driver, a pattern that may reflect a degree of cranial modularity in amphisbaenians, although this hypothesis remains to be tested.

In amphisbaenians, a large component of variation in endocast morphology remains unexplained by phylogeny, size or snout morphology. One potential source of this variation could be intraspecific variability associated with ontogeny. Endocranial shape changes related to growth have been documented across a wide range of vertebrates, including turtles [51], crocodilians [52,53] and birds [54,55]. In amphisbaenians, ontogenetic allometry strongly influences cranial morphology, with the skull typically becoming slenderer and elongate during growth as reported in several species, including *Amphisbaena caeca* [56], *Amphisbaena alba* [31], *Cynisca leucura* [57], *Diplometopon zarudnyi* [58], *Leposternon microcephalum* [59] and species of the genus

Zygaspis [60]. In the specimens examined here, the tight interlocking of the snout bones and the constriction of the parietal posterior to the frontoparietal suture suggest adult stages [57]. However, because the precise ages of the individuals remain unknown, the possibility that part of the observed variation reflects residual ontogenetic signals cannot be excluded. Future studies incorporating growth series or specimens of known age will therefore be necessary to clarify ontogenetic influences on endocranial morphology in amphisbaenians.

Sexual dimorphism may also contribute to intraspecific variation in amphisbaenian endocast morphology. Although its influence on skull morphology remains poorly documented in amphisbaenians, available evidence suggests that it can be significant. For example, females of *Zygaspis quadrifrons* possess larger cranial elements and distinct parietal morphologies [60], whereas males of *T. wiegmanni* have larger heads than females of similar body size [61]. Such differences indicate that sex-related variation could contribute to the residual endocranial variability observed here. Assessing this possibility will require future analyses incorporating sex-specific information and broader intraspecific sampling.

Beyond intraspecific factors, some of the differences observed in amphisbaenian endocast morphology could reflect variation in sensory ecology. For example, differences in the size and shape of the olfactory bulbs and peduncles may indicate variation in vomerolfactory capabilities, which play important roles in prey and predator detection, conspecific recognition, and assessing social cues [62–64]. By contrast, establishing a clear association between the elongation and orientation of the cerebral hemispheres and specific aspects of sensory ecology remains challenging. This region processes multiple functions—including sensory processing, motor coordination, and higher cognitive tasks [65,66]—making it difficult to attribute shape variation to a single factor. To date, no studies have examined how the morphology of the cerebral hemispheres relates to sensory ecology in amphisbaenians, and available data from other squamates provide no clear evidence of such links [49]. Future research combining analyses of the internal organization of squamate cerebral hemispheres with ecological and behavioural data will be essential for clarifying the sources of variability reported here.

Finally, given the close relationships between skull shape and musculature in squamates [67–69], investigating endocast variability in amphisbaenians from a myological perspective could provide valuable insights. The architecture, size and orientation of cranial and neck muscles shape the braincase, which forms the boundaries of the brain cavity and may thus directly constrain the morphology of the enclosed endocast. Analysing muscle architecture, size and fibre orientation, together with ecological variables influencing muscular variation (e.g. diet [69]; soil type [70]), could help identify the biomechanical and ecological factors shaping endocast morphology within Amphisbaenia. To date, detailed information on cranial and neck musculature in this clade is extremely limited, with data available only for *Leposternon microcephalum* [70]. Nevertheless, the promising results obtained using diceCT techniques, as previously applied to shoulder muscles in some amphisbaenians [71], provide a solid foundation for future studies.

In conclusion, while amphisbaenian endocasts display general trends similar to those observed in other fossorial squamates, our comparative analyses across snout morphotypes indicate that extreme cranial modifications related to digging performance do not produce a single, predictable endocast configuration. Taxa sharing the same snout shape exhibit substantial variation in endocast morphology, suggesting that anterior skull modifications influence the braincase only locally rather than deterministically. These results highlight the morphological flexibility of the endocranium under strong functional pressures. Future endocranial studies in both extant and fossil taxa should, whenever possible, interpret morphology within a broad comparative framework to capture multiple sources of variation.

Ethics. This work did not require ethical approval from a human subject or animal welfare committee.

Data accessibility. The electronic supplementary material is available in [72]. The raw geometric morphometric landmark data, specimen classifier file, and R scripts required to reproduce the statistical analyses and figures are available on Zenodo (https://doi.org/10.5281/zenodo.19692110). The newly generated CT image stacks are currently being used in ongoing research and will therefore be made available upon reasonable request to the corresponding author. All endocast surface meshes (.ply files) generated in this study are available on MorphoSource under the project name 'Amphisbaenian endocasts' (https://www.morphosource.org/projects/000839453?locale=en). Supplementary material is available online [72].

Declaration of AI use. We have not used AI-assisted technologies in creating this article.

Authors' contributions. R.A.: conceptualization, investigation, methodology, writing—original draft; E.P.: methodology, writing—review and editing; R.G.: resources, writing—review and editing; M.T.S.: supervision, writing—review and editing; A.H.: supervision, writing—review and editing.

All authors gave final approval for publication and agreed to be held accountable for the work performed therein.

Conflict of interest declaration. We declare we have no competing interests.

Funding. This project was supported by an NSERC Discovery Grant Evolution and Ecology to M.T.S., and two Fundação de Amparoà Pesquisa do Estado de São Paulo grants (FAPESP, 2012/ 24755-8 and 2016/06866-8) to R.G.

Acknowledgements. We would like to acknowledge S. Baumgart, N. Rios, C. Spencer, M. Olson, E. Stanley, G. Pandelis, L. Scheinberg, J. Martinez, J. Maisano, J. Gray, M. Gage, A. Zhang and D. Blackburn for access to CT scans through the Morphosource database. We acknowledge the European Synchrotron Radiation Facility (ESRF) for providing synchrotron radiation facilities. We would like to thank D. Blackburn, G. Ferreira and one anonymous reviewer for the helpful and constructive comments.

References

1. Stayton CT. 2015 What does convergent evolution mean? The interpretation of convergence and its implications in the search for limits to evolution. *Interface Focus* **5**, 20150039. (doi:10.1098/rsfs.2015.0039)
2. Losos JB. 2011 Convergence, adaptation, and constraint. *Evol. Int. J. Org. Evol.* **65**, 1827–1840. (doi:10.1111/j.1558-5646.2011.01289.x)
3. Bergmann PJ, Berry DS. 2021 How head shape and substrate particle size affect fossorial locomotion in lizards. *J. Exp. Biol.* **224**, b242244. (doi:10.1242/jeb.242244)

4. Bergmann PJ, Mann SDW, Morinaga G, Freitas ES, Siler CD. 2020 Convergent evolution of elongate forms in craniates and of locomotion in elongate squamate reptiles. *Integr. Comp. Biol.* **60**, 190–201. (doi:10.1093/icb/icaa015)
5. Sansalone G, Castiglione S, Raia P, Archer M, Dickson B, Hand S, Piras P, Profico A, Wroe S. 2020 Decoupling functional and morphological convergence, the study case of fossorial mammalia. *Front. Earth Sci.* **8**, 112. (doi:10.3389/feart.2020.00112)
6. Wiens JJ, Brandley MC, Reeder TW. 2006 Why does a trait evolve multiple times within a clade? Repeated evolution of snakelike body form in squamate reptiles. *Evol. Int. J. Org. Evol.* **60**, 123–141.
7. Gans C. 1974 *Biomechanics: an approach to vertebrate biology*. Philadelphia, PA: Lippincott Company.
8. Barros FC, Herrel A, Kohlsdorf T. 2011 Head shape evolution in Gymnophthalmidae: does habitat use constrain the evolution of cranial design in fossorial lizards? *J. Evol. Biol.* **24**, 2423–2433. (doi:10.1111/j.1420-9101.2011.02372.x)
9. Anelli V, Bars-Closel M, Herrel A, Kohlsdorf T. 2024 Different selection regimes explain morphological evolution in fossorial lizards. *Funct. Ecol* **38**, 1250–1264. (doi:10.1111/1365-2435.14557)
10. Oliveira BHS, Colli GR, Vitt LJ, Mesquita DO. 2024 Evolution of fossoriality in microteiid lizards. *Zool. J. Linn. Soc.* **201**, e089. (doi:10.1093/zoolinnean/zlae089)
11. de Barros FC, Grizante MB, Zampieri FAM, Kohlsdorf T. 2021 Peculiar relationships among morphology, burrowing performance and sand type in two fossorial microteiid lizards. *Zoology* **144**, 125880. (doi:10.1016/j.zool.2020.125880)
12. Le Guilloux M, Miralles A, Measey J, Vanhooydonck B, O'Reilly JC, Lowie A, Herrel A. 2020 Trade-offs between burrowing and biting force in fossorial scincid lizards? *Biol. J. Linn. Soc.* **130**, 310–319. (doi:10.1093/biolinnean/blaa031)
13. Vanhooydonck B, Boistel R, Fernandez V, Herrel A. 2011 Push and bite: trade-offs between burrowing and biting in a burrowing skink (*Acontias percivali*). *Biol. J. Linn. Soc.* **102**, 91–99. (doi:10.1111/j.1095-8312.2010.01563.x)
14. Boistel R, Herrel A, Lebrun R, Daghfous G, Tafforeau P, Losos JB, Vanhooydonck B. 2011 Shake rattle and roll: the bony labyrinth and aerial descent in squamates. *Integr. Comp. Biol.* **51**, 957–968. (doi:10.1093/icb/icr034)
15. Yi H, Norell MA. 2015 The burrowing origin of modern snakes. *Sci. Adv.* **1**, e1500743. (doi:10.1126/sciadv.1500743)
16. Palci A, Hutchinson MN, Caldwell MW, Lee MSY. 2017 The morphology of the inner ear of squamate reptiles and its bearing on the origin of snakes. *R. Soc. Open Sci.* **4**, 170685. (doi:10.1098/rsos.170685)
17. Yi H. 2022 Using adaptive traits in the ear to estimate ecology of early snakes. In *The origin and early evolutionary history of snakes* (eds DJ Gower, H Zaher), pp. 271–293. Cambridge, UK: Cambridge University Press. (doi:10.1017/9781108938891.018)
18. Camaiti M, Wiles J, Aguilar R, Hutchinson MN, Hipsley CA, Chapple DG, Evans AR. 2023 Ecomorphological correlates of inner ear shape in Australian limb-reduced skinks (Scincidae: Sphenomorphini). *Zool. J. Linn. Soc.* **199**, 994–1012. (doi:10.1093/zoolinnean/zlad074)
19. Latimer AE, Sherratt E, Bonnet T, Scheyer TM. 2023 Semicircular canal shape diversity among modern lepidosaurs: life habit, size, allometry. *BMC Ecol. Evol.* **23**, 10. (doi:10.1186/s12862-023-02113-1)
20. Allemand R, Boistel R, Daghfous G, Blanchet Z, Cornette R, Bardet N, Vincent P, Houssaye A. 2017 Comparative morphology of snake (Squamata) endocasts: evidence of phylogenetic and ecological signals. *J. Anat.* **231**, 849–868. (doi:10.1111/joa.12692)
21. Allemand R, Abdul-Sater J, Macrì S, Di-Poï N, Daghfous G, Silcox MT. 2023 Endocast, brain, and bones: correspondences and spatial relationships in squamates. *Anat. Rec. (Hoboken N J* **306**, 2443–2465. (doi:10.1002/ar.25142)
22. Macrì S, Savriama Y, Khan I, Di-Poï N. 2019 Comparative analysis of squamate brains unveils multi-level variation in cerebellar architecture associated with locomotor specialization. *Nat. Commun.* **10**, 5560. (doi:10.1038/s41467-019-13405-w)
23. Macrì S, Aalto IM, Allemand R, Di-Poï N. 2023 Reconstructing the origin and early evolution of the snake brain. *Sci. Adv.* **9**, i6888. (doi:10.1126/sciadv.adi6888)
24. Scanferla A. 2022 A glimpse into the evolution of the ophidian brain. In *The origin and early evolutionary history of snakes* (eds D Gower, H Zaher), pp. 294–315. Cambridge, UK: Cambridge University Press. (doi:10.1017/9781108938891.019)
25. Kearney M. 2003 Systematics of the Amphisbaenia (Lepidosauria: Squamata) based on morphological evidence from recent and fossil forms. *Herpetological Monographs* **17**, 1. (doi:10.1655/0733-1347(2003)017[0001:SOTALB]2.0.CO;2)
26. Bell CJ, Cadena C, Meza A, Rudie L, Lewis PJ. 2024 Cranial anatomy of the 'round-headed' Amphisbaenian *Zygaspis quadrifrons* (Squamata, Amphisbaenia) based on high-resolution x-ray computed tomography. *Anat. Rec.* **307**, 495–532. (doi:10.1002/ar.25304)
27. Measey GJ, Tolley KA. 2013 A molecular phylogeny for sub-Saharan amphisbaenians. *Afr. J. Herpetol.* **62**, 100–108. (doi:10.1080/21564574.2013.824927)
28. Longrich NR, Vinther J, Pyron RA, Pisani D, Gauthier JA. 2015 Biogeography of worm lizards (Amphisbaenia) driven by end-Cretaceous mass extinction. *Proc. R. Soc. B* **282**, 20143034. (doi:10.1098/rspb.2014.3034)
29. Graboski R, Grazziotin FG, Mott T, Trefaut Rodrigues M. 2022 The phylogenetic position of ridley's worm lizard reveals the complex biogeographic history of New World insular amphisbaenids. *Mol. Phylogenetics Evol.* **173**, 107518. (doi:10.1016/j.ympev.2022.107518)
30. Gans C. 1978 The characteristics and affinities of the Amphisbaenia. *Trans. Zool. Soc. Lond.* **34**, 347–416. (doi:10.1111/j.1096-3642.1978.tb00376.x)
31. Gans C, Montero R. 2008 An atlas of amphisbaenian skull anatomy. In *Biology of the reptilia, volume 21, morphology I: the skull and appendicular locomotor apparatus of Lepidosauria* (eds C Gans, AS Gaunt, K Adler), pp. 621–738. Ithaca, NY: Society for the Study of Amphibians and Reptiles.
32. Kearney M, Stuart BL. 2004 Repeated evolution of limblessness and digging heads in worm lizards revealed by DNA from old bones. *Proc. R. Soc. B* **271**, 1677–1683. (doi:10.1098/rspb.2004.2771)
33. Blackburn DC *et al*. 2024 Increasing the impact of vertebrate scientific collections through 3D imaging: the openvertebrate (oVert) thematic collections network. *Bioscience* **74**, 169–186. (doi:10.1093/biosci/biad120)
34. Boyer DM, Gunnell GF, Kaufman S, McGeary TM. 2016 Morphosource: archiving and sharing 3-D digital specimen data. *Paleontol. Soc. Pap.* **22**, 157–181. (doi:10.1017/scs.2017.13)
35. Masschaele B, Dierick M, Loo DV, Boone MN, Brabant L, Pauwels E, Cnudde V, Hoorebeke LV. 2013 HECTOR: A 240kV micro-CT setup optimized for research. *J. Phys.* **463**, 012012. (doi:10.1088/1742-6596/463/1/012012)
36. Allemand R, López-Aguirre C, Abdul-Sater J, Khalid W, Lang MM, Macrì S, Di-Poï N, Daghfous G, Silcox MT. 2023 A landmarking protocol for geometric morphometric analysis of squamate endocasts. *Anat. Rec.* **306**, 2425–2442. (doi:10.1002/ar.25162)
37. Baken EK, Collyer ML, Kaliontzopoulou A, Adams DC. 2021 geomorph v4.0 and gmShiny: enhanced analytics and a new graphical interface for a comprehensive morphometric experience. *Methods Ecol. Evol.* **12**, 2355–2363. (doi:10.1111/2041-210x.13723)
38. Revell LJ. 2012 phytools: an R package for phylogenetic comparative biology (and other things). *Methods Ecol. Evol.* **3**, 217–223. (doi:10.1111/j.2041-210x.2011.00169.x)

39. Adams DC. 2014 A generalized K statistic for estimating phylogenetic signal from shape and other high-dimensional multivariate data. *Syst. Biol.* **63**, 685–697. (doi:10.1093/sysbio/syu030)
40. Schliep KP. 2011 phangorn: phylogenetic analysis in R. *Bioinformatics* **27**, 592–593. (doi:10.1093/bioinformatics/btq706)
41. Clavel J, Escarguel G, Merceron G. 2015 mvmorph: an r package for fitting multivariate evolutionary models to morphometric data. *Methods Ecol. Evol.* **6**, 1311–1319. (doi:10.1111/2041-210x.12420)
42. Clavel J, Morlon H. 2020 Reliable phylogenetic regressions for multivariate comparative data: illustration with the MANOVA and application to the effect of diet on mandible morphology in phyllostomid bats. *Syst. Biol.* **69**, 927–943. (doi:10.1093/sysbio/syaa010)
43. Guillerme T *et al*. 2020 Disparities in the analysis of morphological disparity. *Biol. Lett.* **16**, 20200199. (doi:10.1098/rsbl.2020.0199)
44. Guillerme T. 2018 dispRity: a modular R package for measuring disparity. *Methods Ecol. Evol.* **9**, 1755–1763. (doi:10.1111/2041-210x.13022)
45. Bhattacharyya A. 1946 On a measure of divergence between two multinomial populations. *Sankhyā: Indian J. Stat.* **7**, 401–406.
46. Castiglione S *et al*. 2019 A new, fast method to search for morphological convergence with shape data. *PLoS One* **14**, e0226949. (doi:10.1371/journal.pone.0226949)
47. Melchionna M *et al*. 2021 A method for mapping morphological convergence on three-dimensional digital models: the case of the mammalian sabre-tooth. *Palaeontology* **64**, 573–584. (doi:10.1111/pala.12542)
48. Allemand R, Polcyn MJ, Houssaye A, Vincent P, López-Aguirre C, Bardet N. 2024 First virtual reconstruction of a mosasaurid brain endocast: description and comparison of the endocast of tethysaurus nopcsai with those of extant squamates. *Diversity* **16**, 548. (doi:10.3390/d16090548)
49. Segall M, Cornette R, Rasmussen AR, Raxworthy CJ. 2021 Inside the head of snakes: influence of size, phylogeny, and sensory ecology on endocranium morphology. *Brain Struct. Funct.* **226**, 2401–2415. (doi:10.1007/s00429-021-02340-6)
50. Araújo Salvino C, Hernandéz-Morales C, Daza JD, Nunes PMS. 2024 Comparative anatomy and evolution of the atlantoaxial complex in the fossorial lineage Amphisbaenia (Squamata: Lacertoidea). *Anat. Rec. (Hoboken N J* **307**, 3623–3648. (doi:10.1002/ar.25448)
51. Ferreira GS, Werneburg I, Lautenschlager S, Evers SW. 2022 Contrasting brains and bones: neuroanatomical evolution of turtles (Testudinata). In *Paleoneurology of amniotes: new directions in the study of fossil endocasts* (eds MT Dozo, A Paulina-Carabajal, TE Macrini, S Walsh), pp. 79–121. Cham, Switzerland: Springer. (doi:10.1007/978-3-031-13983-3_4)
52. Jirak D, Janacek J. 2017 Volume of the crocodilian brain and endocast during ontogeny. *PLoS One* **12**, e0178491. (doi:10.1371/journal.pone.0178491)
53. Hu K, King JL, Romick CA, Dufeau DL, Witmer LM, Stubbs TL, Rayfield EJ, Benton MJ. 2021 Ontogenetic endocranial shape change in alligators and ostriches and implications for the development of the non-avian dinosaur endocranium. *Anat. Rec.* **304**, 1759–1775. (doi:10.1002/ar.24579)
54. Kawabe S, Shimokawa T, Miki H, Matsuda S, Endo H. 2013 Variation in avian brain shape: relationship with size and orbital shape. *J. Anat.* **223**, 495–508. (doi:10.1111/joa.12109)
55. Kawabe S, Matsuda S, Tsunekawa N, Endo H. 2015 Ontogenetic shape change in the chicken brain: implications for paleontology. *PLoS One* **10**, e0129939. (doi:10.1371/journal.pone.0129939)
56. Magwene PM. 1996 Patterns of cranial growth in the worm-lizard, Amphisbaena caeca. *Am. Zool* **36**, 53–64.
57. Hipsley CA, Rentinck MN, Rödel MO, Müller J. 2016 Ontogenetic allometry constrains cranial shape of the head-first burrowing worm lizard *Cynisca leucura* (Squamata: Amphisbaenidae). *J. Morphol.* **277**, 1159–1167. (doi:10.1002/jmor.20564)
58. Hawkins RK, Bell CJ, Olori JC, Stocker MR. 2022 Intraspecific variation in the cranial osteology of *Diplometopon zarudnyi* (Squamata: Amphisbaenia: Trogonophidae). *J. Morphol.* **283**, 1359–1375. (doi:10.1002/jmor.21508)
59. Hohl L dos SL, Azorit C, Vassallo AI, Casinos A, Machado AS, Lopes RT, Rocha-Barbosa O. 2023 Ontogenetic skull variation in a shovel-headed amphisbaenian species. *J. Morphol.* **284**, e21643. (doi:10.1002/jmor.21643)
60. Meza A, Bell CJ, Daza JD, Thies ML, Lewis PJ. 2024 Variation in the cranial osteology of the amphisbaenian genus *Zygaspis* based on high-resolution x-ray computed tomography. *Anat. Rec.* **307**, 475–494. (doi:10.1002/ar.25321)
61. Martín J, Polo-Cavia N, Gonzalo A, López P, Civantos E. 2012 Sexual dimorphism in the north african amphisbaenian *Trogonophis wiegmanni*. *J. Herpetol.* **46**, 338–341. (doi:10.1670/10-286)
62. López P, Martín J. 2001 Chemosensory predator recognition induces specific defensive behaviours in a fossorial amphisbaenian. *Anim. Behav.* **62**, 259–264. (doi:10.1006/anbe.2001.1762)
63. Martín J, Raya García E, Ortega J, López P. 2020 How to maintain underground social relationships? Chemosensory sex, partner and self recognition in a fossorial amphisbaenian. *PLoS One* **15**, e0237188. (doi:10.1371/journal.pone.0237188)
64. Martín J, Raya-García E, Ortega J, López P. 2021 Offspring and adult chemosensory recognition by an amphisbaenian reptile may allow maintaining familiar links in the fossorial environment. *PeerJ* **9**, e10780. (doi:10.7717/peerj.10780)
65. Donkelaar HJ. 1998 Reptiles. In *The central nervous system of vertebrates* (eds R Nieuwenhuys, HJ Donkelaar, C Nicholson), pp. 1315–1499. Berlin, Germany: Springer-Verlag. (doi:10.1007/978-3-642-18262-4_20)
66. Butler AB, Hodos W. 2005 *Comparative vertebrate anatomy: evolution and adaptation*. Hoboken, NJ: John Wiley & Sons.
67. Fabre AC, Andrade DV, Huyghe K, Cornette R, Herrel A. 2014 Interrelationships between bones, muscles, and performance: biting in the lizard tupinambis merianae. *Evol. Biol.* **41**, 518–527. (doi:10.1007/s11692-014-9286-3)
68. Watanabe A, Fabre AC, Felice RN, Maisano JA, Müller J, Herrel A, Goswami A. 2019 Ecomorphological diversification in squamates from conserved pattern of cranial integration. *Proc. Natl. Acad. Sci. USA* **116**, 14688–14697. (doi:10.1073/pnas.1820967116)
69. Taverne M, Watson PJ, Dutel H, Boistel R, Lisicic D, Tadic Z, Fabre AC, Fagan MJ, Herrel A. 2023 Form-function relationships underlie rapid dietary changes in a lizard. *Proc. R. Soc. B* **290**, 20230582. (doi:10.1098/rspb.2023.0582)
70. Navas CA, Antoniazzi MM, Carvalho JE, Chaui-Berlink JG, James RS, Jared C, Kohlsdorf T, Pai-Silva MD, Wilson RS. 2004 Morphological and physiological specialization for digging in amphisbaenians, an ancient lineage of fossorial vertebrates. *J. Exp. Biol.* **207**, 14. (doi:10.1242/jeb.01041)
71. Westphal N, Mahlow K, Head JJ, Müller J. 2019 Pectoral myology of limb-reduced worm lizards (Squamata, Amphisbaenia) suggests decoupling of the musculoskeletal system during the evolution of body elongation. *BMC Evol. Biol.* **19**, 16. (doi:10.1186/s12862-018-1303-1)
72. Allemand R, Patterson E, Graboski R, Silcox MT, Herrel A. 2026 Supplementary material from: Endocranial morphology in worm lizards (Amphisbaenia, Squamata): multiple neuroanatomical solutions to a fossorial lifestyle. Figshare. (doi:10.6084/m9.figshare.c.8516961)